Chin. J. Astron. Astrophys. Vol. 7 (2007), No. 1, 129–140
(*http://www.chjaa.org*)

Chinese Journal of
Astronomy and
Astrophysics

Eruption of an Active-Region Filament Driven by an Emerging Bipole *

Yun-Chun Jiang[1], Yuan-Deng Shen[1] and Jing-Xiu Wang[2]

[1] National Astronomical Observatories / Yunnan Observatory, Chinese Academy of Sciences, Kunming 650011; *jyc@ynao.ac.cn*

[2] National Astronomical Observatories, Chinese Academy of Sciences, Beijing 100012

Received 2006 July 29; accepted 2006 November 1

Abstract A section of an S-shaped filament underwent an eruption in a sigmoidal active region (AR 8027) with S-shaped coronal structure, which was clearly driven by a bipole emerging below the NW end of the filament. The bipole with two separating poles showed typical characteristics of emerging flux region (EFR) and its axis rotated counterclockwise. Two cancelling magnetic features (CMFs) were formed between the two poles and adjacent flux with opposite polarity and substantial flux cancellation occurred in them. Along with the bipole emergence the filament was strongly disturbed. Just before the filament eruption, two X-ray loops overlying the filament brightened, an axial X-ray structure and then a cusp structure appeared. During the eruption first the whole filament rose and then its SE end broke away from the chromosphere, while its NW end remained stationary. Helical structure and motion were observed in the filament body and downward mass motion in the two ends. After the eruption, a major part of the filament remained and slowly returned to quiescence, and an X-ray arcade and an axial structure formed. These observations suggest that the eruption resulted from the interaction between the bipole and the overlying loops. We provide evidence that steady photospheric reconnection between their footprints took place in the two CMFs during the bipole emergence.

Key words: Sun: filaments — Sun: flares — Sun: magnetic fields — Sun: corona — Sun: X-rays

1 INTRODUCTION

Filaments are cool, dense material suspended in the hot, tenuous corona. It is widely accepted that the global magnetic field surrounding the filaments plays a key role in their formation, structure and stability (Tandberg-Hanssen 1995). Filaments are always located above polarity inversions of photospheric magnetic field and beneath coronal arcades connecting opposite polarity regions; their formation and existence are closely related to the development of the axial field (Martin 1998). Generally, filaments are steadily supported by magnetic field and so develop slowly. Sometime, however, they are strongly disturbed and are observed to disappear. These disappearances can be thermal or dynamical (filament eruptions) (Mouradian et al. 1995). Filament eruptions are spectacular phenomena, usually associated with two-ribbon flares, coronal mass ejections (CMEs), and formations of X-ray bright arcades (Tandberg-Hanssen 1995; McAllister et al. 1996; Khan et al. 1998; Uchida 1998). During the eruptions, helical structure and motion are frequently observed (Schmieder et al. 1985; Raadu et al. 1988; Rompolt 1990; Vršnak et al. 1991; Wang et al. 1996a; Jiang & Wang 2000, 2001), but their formation and development are still not well understood.

* Supported by the National Natural Science Foundation of China.

Observations of helically eruptive filaments not only provide an insight into the structure, dynamics and magnetic field configuration of filaments in general, but also can help us to understand such related violent processes as flares and CMEs, etc. The cause of filament instability is another important but unresolved problem (Fillippov 1998). Photospheric displacement and changes of photospheric magnetic field near the filaments may greatly contribute to loss of filament stability. Previous studies have shown that filament disturbances are closely related to pore birth and movement, flux emergence and cancellation (Rust et al. 1975; Simon et al. 1986; Raadu et al. 1988; Moore & Roumeliotis 1992; Martin & Livi 1992; Feynman & Martin 1995; Wang et al. 1996a; Wang & Sheeley 1999; Jiang & Wang 2000, 2001; Zhang, Wang & Nitta 2001; Kim et al. 2001; Jiang, Li & Yang 2006). Obviously, observations of interaction between emerging bipoles and filaments are important for a better understanding of the conditions of the onset and growth of filament instability.

In this paper we concentrate on the eruption of an S-shaped filament and its associated subflare in the sigmoidal active region, AR 8027, that occurred on 1997 April 9. The eruption was clearly triggered by an emerging bipole, and helical structure and motion were observed during the eruption. Filtergrams, Dopplergrams and magnetograms of the chromosphere and photosphere were taken by the Multi-Channel Solar Telescope (MCST) installed at Huairou Solar Observing Station (HSOS) of the National Astronomical Observatories. In addition, 195 Å and soft X-ray images were obtained by the Extreme-ultraviolet Images Telescope (EIT) on board Solar and Heliospheric Observatory (SOHO) and the Soft X-ray Telescope (SXT) on board the Yohkoh satellite. These observations enable us to study the response of the filament to the emerging bipole and the physical relationship between the new flux, filament eruption and subflare.

2 OBSERVATIONS

2.1 Instrument

The MCST consists of five telescopes, including the 14 cm H_α Telescope and the 35 cm Solar Magnetic Field Telescope (SMFT) (Deng et al. 1997). For the present study, the following data of MCST are used. (a) H_α line center images taken by the 14 cm H_α Telescope with a field of view (FOV) of $12.8' \times 8.0'$. (b) Magnetograms, filtergrams and Dopplergrams of the photosphere obtained by SMFT (Ai & Hu 1986). The longitudinal field was measured in the blue wing of Fe 5324, 0.075 Å from the line center, and the transverse field was measured in the line center of Fe 5324. The noise level for line-of-sight magnetograms with 255 pairs of integration is about 15 G, while for the transverse field measurement, it is less than 150 G. Wang et al.(1996b) have given detailed descriptions for the calibration and data reductions of the photospheric magnetograms. The chromospheric (photospheric) line-of-sight velocity fields in H_β (Fe 5324) line were measured with the subtraction technique at $\pm$0.24 Å ($\pm$0.15 Å) from the line center. The Dopplergram calibration was based on the solar rotation, which was described by Wang et al. (1996a). To obtain the detailed Dopplergrams, we have eliminated the solar rotation and steady flows by subtracting a large-scale, smoothed background obtained from the raw Dopplergrams (Wang 1993). The spatial resolution is 2–3 arcsec for both Dopplergrams and photospheric magnetograms.

The Yohkoh/SXT was described by Tsuneta et al. (1991). Yohkoh missed the data for the main eruption phase, but both full frame images (FFIs) and partial frame images (PFIs) were obtained for the pre- and post-eruption phase. The SOHO/EIT obtained full-disk images roughly every 12 to 15 min with a pixel resolution of $2.6''$ in the Fe XII band 195 Å emission line (for details see Delaboudiniére et al. 1995). For the present study the SOHO/MDI (the Michelson Doppler Imager) full-disk magnetograms with a 96-minute cadence are also examined.

The coalignment between different datasets was done by coaligning common features in the different images. The full-disk SXT to EIT coalignment was done by fitting the solar limbs. Then, the MDI magnetograms were used to match SXT FFIs, HSOS H_α/H_β images and magnetograms with full-disk SXT and EIT 195 Å images, by means of sunspots, H_α and soft X-ray features.

2.2 General Evolution of Active Region and Filament

AR 8027 was a small decaying region. It appeared from the eastern limb on April 4, then gradually dispersed and completely disappeared on the solar disk on April 11 (Solar–Geophysical Data, No.634, Part I, 1997). On April 9, the region was near its central meridian passage (S28E00). The observed filament eruption

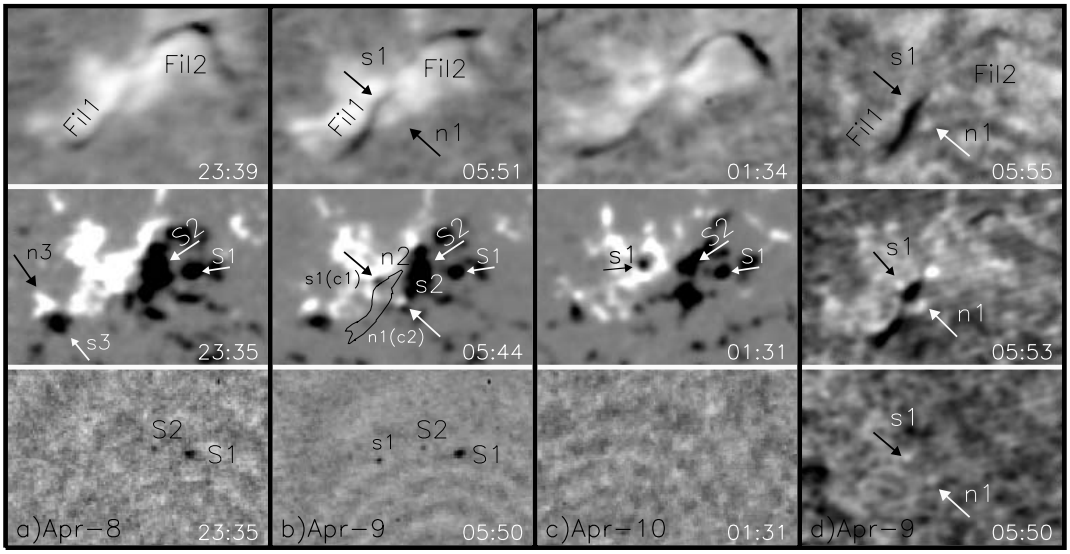

Fig. 1 General appearance of AR 8027 before (a) and after (b), (d) the filament eruption on April 9 and on April 10 (c). In (a), (b) and (c), the panels from top to bottom are H_α line center images, line-of-sight magnetograms and Fe5324Å/0.150Å filtergrams of photosphere, respectively, and in (d), offband H_β/0.125Å filtergram, H_β Dopplergram and Fe5324 Dopplergram. In the magnetogram at 05:44 UT, the H_β filament was superposed as black contour. In the Dopplergrams, the black (white) patches represent blueshifts (redshifts). The two arrows in the filtergrams and Dopplergrams mark the two poles of the emerging bipole. North is up and west to right. The FOV is $190'' \times 130''$.

occurred around 04:25 UT, and an associated subflare of X-ray class B4.2 had peak time around 04:34 UT. Figure 1 shows the general appearance of the region before (Fig. 1(a)) and after (Fig. 1(b) and 1(d)) the eruption on April 9, and on the next day (Fig. 1(c)). The preceding end of AR 8027 consisted of two small sunspots of negative polarity, S1 and S2; the following end was an enhanced network with positive polarity. In the Fe 5324 Å filtergrams, S1 and S2 decreased in size from April 8 to 9 and then disappeared on April 10. Figure 1 shows that two filaments, Fil1 and Fil2, formed an overall S-shape between the preceding and following ends of AR 8027. The filament that erupted on April 9 was the SE one, the J-shaped Fil1, so we only focus on it. The most remarkable feature of AR 8027 is that it was a sigmoidal active region (Rust & Kumar 1996; Canfield et al. 1999). In their study of the X-ray dimming associated with a Halo CME on April 7, Sterling & Hudson (1997) showed that a bright S-shaped X-ray structure was predominant in this region.

The most distinct photospheric activity on April 9 was a bipole emerging just below the NW end of Fil1. When its two poles, n1 and s1, first appeared at 02:01 UT, they had collided with the existing flux with polarities opposite to them, n1 with s2 and s1 with n2. Thus two cancelling magnetic features (CMFs), c1 and c2, were formed. The bipole emergence and its forced flux cancellation were fairly obvious in the magnetograms of Figure 1. In both H_β and Fe 5324Å Dopplergrams after the eruption, we note that two redshift cells (indicated by the two arrows) appeared just at the sites of the two poles. In the Fe 5324 Å filtergrams, only s1 showed up as a pore while n1 did not. By April 10, s1 became a parasitic polarity surrounded by positive network, while n1 had already completely disappeared in the magnetograms.

The subflare and the eruption occurred at the early phase of the emerging bipole. When the flux emergence and cancellation were underway, the filament was activated and eventually erupted. However, the filament did not completely disappear after the eruption; it still remained by the next day.

3 FILAMENT ERUPTION

3.1 Morphology

About 2.5 h after the bipole appearance, the filament underwent a splendid eruption between about 04:25 and 05:15 UT, as shown by the time sequences of EIT 195 Å and H_α images in Figures 2(a) and 2(b), respectively.

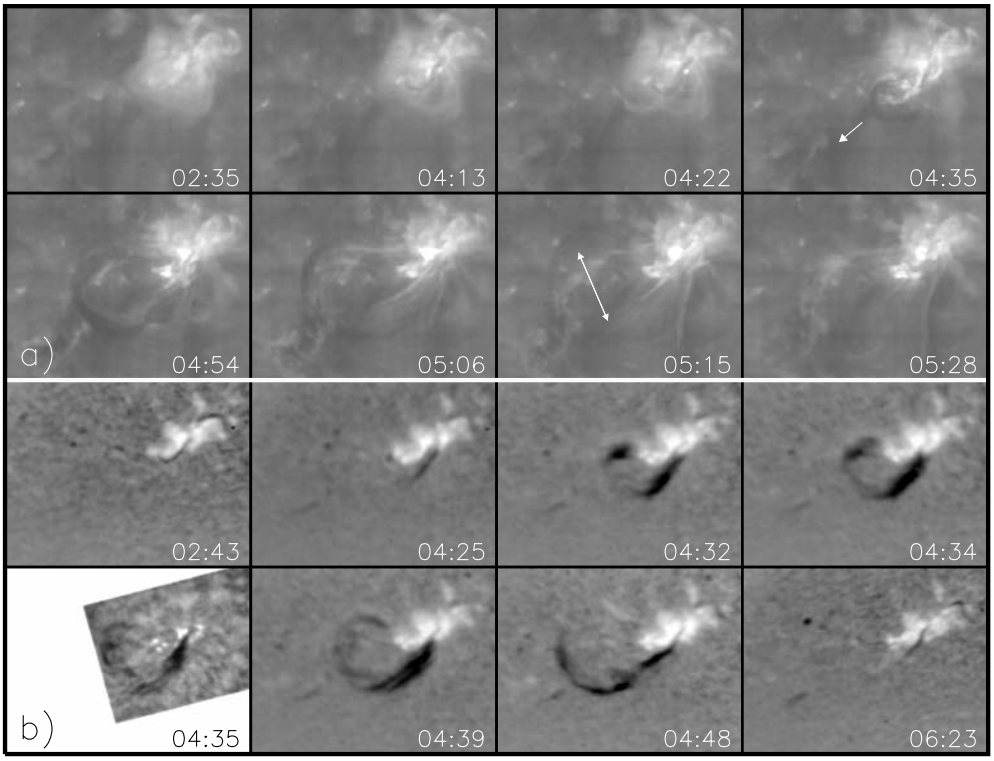

Fig. 2 Time sequences of EIT 195Å (a) and H_α line center (b) images showing the filament eruption. In (b), the frame at 04:35 UT is an H_β image. The white arrow with single head marks the rising direction of the erupting filament, and the white arrow with two heads, the expanding direction of its axis. The FOV is $420'' \times 330''$.

The sudden eruption was first seen at 04:25 UT in H_α and at 04:35 UT in 195 Å. The filament top quickly lifted while its two ends were fixed in the chromosphere (see the white arrow in 195 Å image at 04:35 UT). Simultaneously, its axis swelled perpendicular to the rising direction (see the white arrow with two heads in 195Å image at 05:15 UT). As a result, the erupting filament was shaped like a rising Ω loop. Note that the rise of the top was concentrated in the SE direction. Then, its SE end detached from the chromosphere while the NW end remained rooted (see the H_α image at 04:48 UT). Therefore, the eruption was asymmetrical in shape. Similar examples have been observed (Mouradian et al. 1998; Jiang & Wang 2001). Since the active region was near its central meridian passage in the south hemisphere, and the erupting filament was away from the Sun center in the SE direction, taking the project effect into account, we visualize that the filament did not erupt vertically but had a inclined path, just like the example shown by McAllister et al. (1996). During the eruption helical structure was observed in the H_α/H_β images (see the H_α image at 04:39 UT), suggesting the appearance of helical magnetic field in it. Unfortunately, we cannot trace the development of this structure because of the low cadence of our H_α and H_β observations.

3.2 Dynamics

Figure 3 shows the dynamic characteristics of the emerging bipole and the disturbed filament with time sequences of offband H_β filtergrams (the first, third and fifth rows) and simultaneous Dopplergrams (the second, fourth and sixth rows) before (Fig. 3(a)), during (Fig. 3(b)) and after (Fig. 3(c)) the eruption. Regarding 02:01 UT as the starting time of the bipole emergence, we first describe the Doppler signal of the bipole, then considering the appearance of Dopplershift that did not exist at earlier times as evidence of filament activation, we discuss the dynamics of the filament.

As is usual with EFRs (emerging flux regions), two redshift cells began to appear at the sites of the bipole's two poles (see the black arrows) at 03:43 UT, and persisted until 06:31 UT. This indicates there

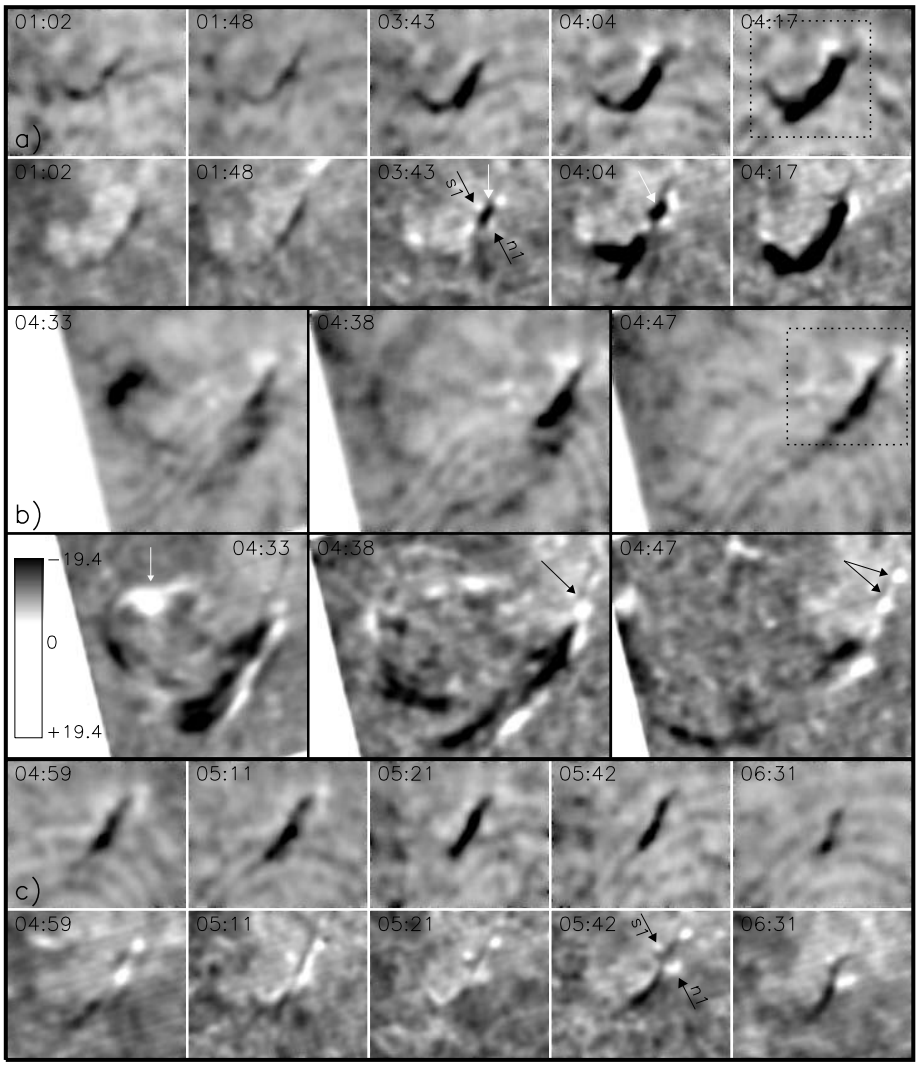

Fig. 3 Time sequences of offband H_β filtergrams (the first, third and fifth rows) and H_β Dopplergrams (the second, fourth and sixth rows) show the filament dynamics before (a), during (b) and after (c) the eruption. The FOV is $145'' \times 110''$ for (a) and (c), and $240'' \times 165''$ for (b). The dashed windows in the frames at 04:17 and 04:47 UT mark the same area, and a scale bar to the Dopplergrams is given in the frame at 04:33 UT.

was chromospheric downflow at the footpoints of the rising flux tube (Zwaan 1987); similar downflow was also observed in the photosphere (see the previous section). On the other hand, a rising of the top of the flux tube was suggested by the appearance of a blueshift patch between the two redshift cells at 03:43 and 04:04 UT (see the white arrows). Note these redshifts and blueshifts did not appear at 01:02 and 01:48 UT before the bipole emerged.

At 01:02 and 01:48 UT, the filament was slender and simply showed faint blueshifts. At 03:43 UT about 90 min after the first appearance of the bipole, however, the filament was clearly activated, as indicated by the presence of weak redshift in its body. Then at 04:04 and 04:17 UT, before the violent eruption, the filament showed strong blueshift; this possibly indicates it began to accelerate. In the filtergrams, the filament showed a tendency of getting thicker from 03:43 to 04:17 UT, suggesting the appearance of either enhanced microturbulence or helical motion (Schmieder et al. 1991).

From 04:33 to 04:47 UT, the filament underwent radial eruption. The H_β filtergrams revealed the same process as the H_α and 195 Å observations. Note that helical structure appeared at 04:33 and 04:38 UT. In the Dopplergrams, a noticeable characteristic of the eruption was the appearance of redshift patches at the two filament ends (see the arrows), suggesting that the filament mass was drained from its rising part towards the two ends. Another remarkable feature was the appearance of alternating blue and red shift streaks along the filament axis, which implies presence of helical motion when the filament erupted upward (Schmieder et al. 1985; Raadu et al. 1988).

After the eruption, a major part of the filament still remained in existence, but the fishhook-like part near the SE end disappeared. This possibly resulted from mass flowing out of the filament down the chromosphere or up into the corona. From 04:59 to 05:21 UT, the filament continued in activating status, with a faint redshift and a major blueshift. Contrary to the situation before the eruption, however, the filament became fainter and fainter, indicating a decreasing internal motion. Then from 05:42 to 06:31 UT, the filament tended towards quiescence and showed mainly faint blueshift again.

In summary, the filament had been disturbed at least 40 min before its eruption. Downward draining mass motion and helical motion appeared during the eruption, and it is evident that part of the filament disappeared. After the eruption, the filament disturbance gradually weakened, and finally the whole filament returned to quiescent state.

3.3 Coronal Evolution

Yohkoh missed the main phase of the subflare, but interesting coronal changes were observed before and after the eruption. In Figures 4(a) and 4(b), the time evolution of the related X-ray structures is shown by PFIs and FFIs of SXT. To aid matching some HSOS images are also included in Figure 4(a) and labeled as "HSOS" (the X-ray images, as "SXT"). The second panel in the first (second) row is the HSOS H_β (H_α) filtergram.

Before the eruption there was a clear bright S-shaped structure of X-ray loops lying above Fil1 and arching over a larger part of the active region. These loops rooted their eastern endpoints in the following polarity, passed over the Fil1 to the northwest and then connected with the preceding polarity. The evolution of soft X-ray structures can be broken down into the following consecutive stages. (1) After a Yohkoh night between about 02:49 and 03:28 UT, a small bright loop, L1 (see the image at 04:13 UT), and a large fainter loop, L2 (see the image at 04:20 UT), appeared to overlay the NW end of the filament. (2) Then a bright thin axial structure beneath L2 was visible along the H_α filament (see the images at 04:21 and 04:22 UT). Similar straight long features were previously observed above stable or erupting H_α filaments (Soberg & McAllister 1998), and were described as "string" by Kano et al. (1994) and "rail" by Khan et al. (1994). Kano et al. (1994) explained the string/rail features as the locus of a series of reconnection points of loops or as the heating points of H_α filament material. (3) Shortly the string/rail structure disappeared, but several cusp-like loops developed from earlier uncusped loops (see the SXT images at 04:22 and 04:26 UT). Previous studies have shown that cusp structures were often associated with eruptive filaments (Tonooka et al. 1998). Due to the appearance of the string/rail structure prior to cusp structure, following the suggestion of Khan et al. (1998), the string/rail feature was possibly related to the axial field structure of the filament in X-ray, while the cusp structure possibly resulted from an interaction between the magnetic field of the filament and the overlying loop.

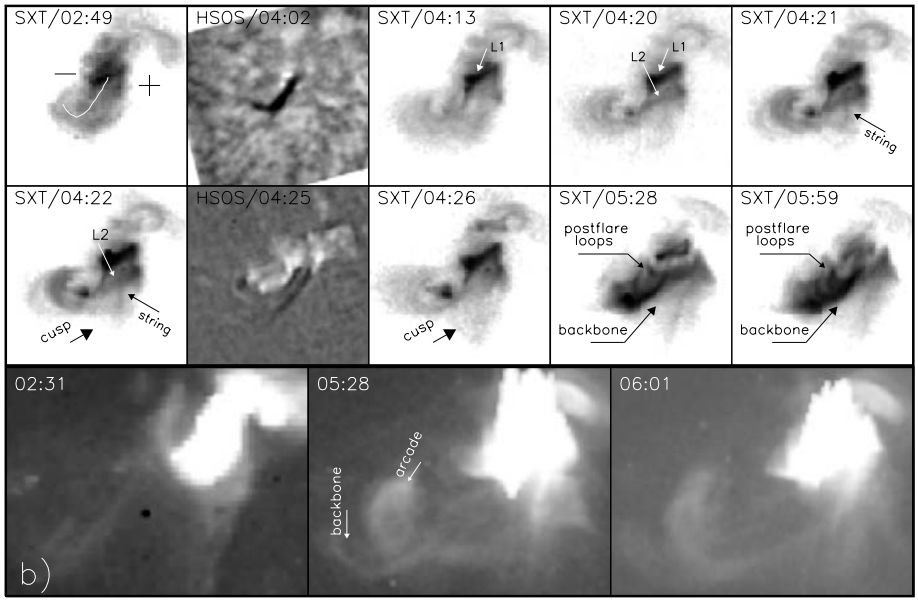

Fig. 4 (a) PFIs (labeled as "SXT") and (b) extracted images from FFIs taken by YOHKOH/SXT show evolution of the coronal structure related to the eruption. Two HSOS H_β and H_α images are also present in (a) (labeled "HSOS"). All of SXT PFI images are shown as negative images, and the white curve in the frame at 02:49 UT represents the axis of H_α/H_β filament. The FOV is $220'' \times 220''$ for (a) and $470'' \times 360''$ for (b).

The filament eruption was over after another Yohkoh night. A bright arcade-like structure consisting of loops appeared and spanned most of the filament site. In addition, a diffuse bright axial structure formed in the west side of the arcade (see the images at 05:28 and 05:59 UT). Similar axial features were also observed in some filament eruption and arcade formation events, and were named "backbone" by McAllister et al. (1992) and "spine" by Uchida (1998) . Examining the FFIs, we also found a backbone structure beneath a large-scale arcade around 05:28UT. By 06:01 UT, the backbone faded away while the arcade was still visible (see Fig. 4(b)).

Taking the maintenance of the filament after the eruption into account, the above observations give us an impression that both of the string/rail and the spine/backbone were associated with the axial field of the filament so represented the X-ray counterpart of the cold H_α filament.

4 BIPOLE EMERGENCE

In Figure 5(a), the relationship between the disturbed filament and the emerging bipole is shown by the time sequence of longitudinal magnetograms in the photosphere with the relevant H_β or H_α filament superposed as white contours. Figure 5(b) presents the vector magnetograms of an area containing only the bipole to exhibit its detailed evolution. The area is marked by the black dashed boxes in the last two frames of Figure 5(a) and magnified by a factor of 3.

The earliest signals of the bipole showed are the two opposite polarity poles at 02:01 UT (see the two arrows). The preceding pole (s1) was northeast of the following pole (n1), and they were located on the two sides of the NW end of the filament. After their appearance, the two poles showed the following remarkable features: (a) As a normal features associated with an EFR, their separation increased very significantly over a time span of about 6h, from 7000 km at 02:01 UT to 22 000 km at 08:01 UT. (b) Their axial direction, from n1 to s1, obviously rotated counterclockwise. The angle between the EFR axis and the south-north direction (marked by the two arrows in frames at 03:34 and 05:44 UT in Fig. 5(b)) continuously increased by about

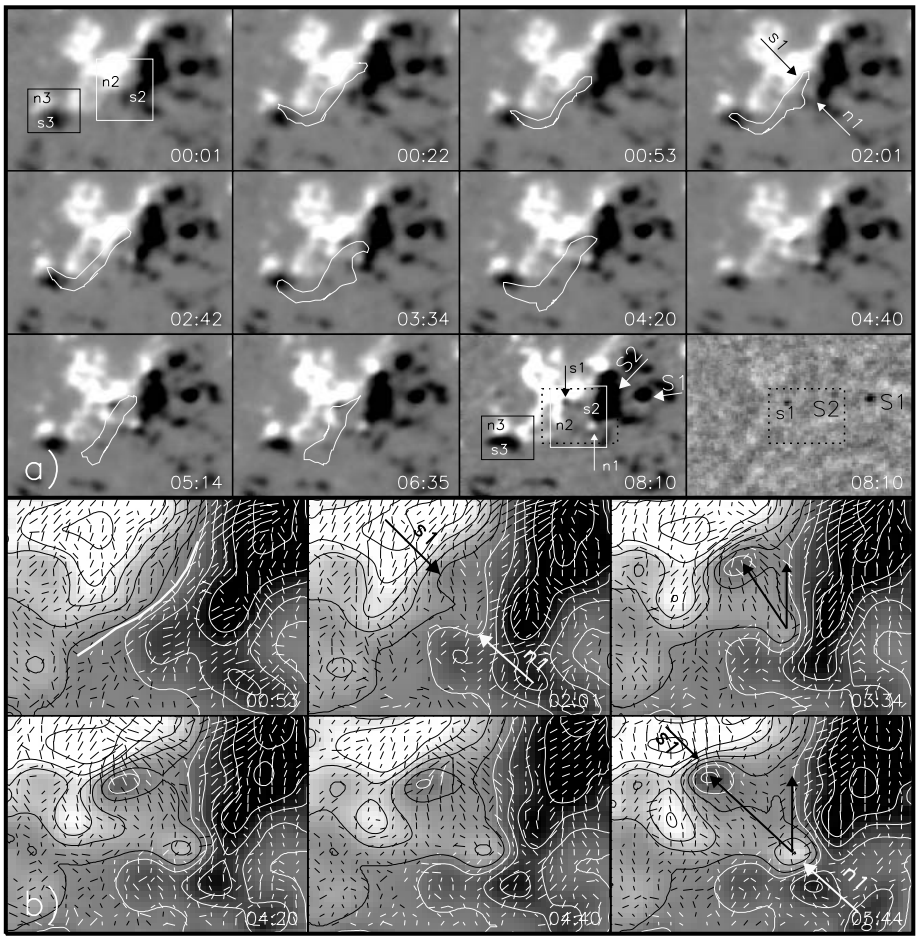

Fig. 5 (a) Time sequences of longitudinal magnetograms in the photosphere. The last frame is an Fe 5324Å/0.150Å filtergram. The field strength is truncated above absolute magnitude 200 G and the FOV is $165'' \times 120''$. (b) A series of enlarged vector magnetograms in the photosphere. The longitudinal components are shown by black (white) isogauss contours for positive (negative) polarities over the grey scale background; the contour levels are $\pm$20, 50, 100 and 200 G. The transverse components are represented by short line segments with lengths proportional to the relative field strength and aligned to the field direction. The black dashed windows in (a) correpond to the FOV of (b).

34° over an interval of less than 4 h, from 3° at 02:01 UT to 36° at 05:55 UT, and then remained nearly unchanged. This rotation might be related to the dynamo action that formed the emerging flux. As shown by Leka et al. (1996), the rotation was consistent with the emergence of a current-carrying flux loop, a kink deformed by the current it carried. (c) They had no sooner appeared than they separately cancelled with adjacent flux of opposite polarity, n1 with s2 and s1 with n2, so two CMFs (c1 and c2) were formed. Due to the spreading motion, they ate away the opposite polarity flux standing in the way so a clear gap empty of flux was formed between them. This flux cancellation obviously continued throughout the emergence of the bipole. Beneath the other end of the filament, however, the two network field features (s3 and n3; also see Fig. 1) showed no clear changes. To determine the actual disappearance of flux in s2 and n2, we first measured the negative (positive) flux in an area including the two poles (marked by the white solid boxes in Fig. 5(a)), then the flux value of the negative (positive) pole was subtracted. To determine whether

or not s3 and n3 played a role in the filament disturbance, we also measured the negative (positive) flux changes in an area including s3 and n3 (marked by the black solid boxes in Fig. 5(a)). Figure 6(a) shows the changes of photospheric magnetic flux in the two poles, and Figure 6(b), in s2, n2, s3 and n3. Throughout the observational period, the flux in s1 and n1 first increased and then gradually decreased, while in s2 and n2, continuously decreased. In s3 and n3, however, the flux stayed nearly unchanged. Therefore, the eruption should be mainly related to the bipole emergence and its forced flux cancellation, while it had no direct relationship with s3 and n3 although the SE filament end detached from the chromosphere during the eruption. (d) Only s1 appeared as a pore and n1 did not (see Sect.2). In the photospheric filtergrams, the pore first appeared at 03:34 UT and then persisted until the end of observation (see Fig. 1 and the last frame in Fig. 5(a)).

Figures 6(a) and 6(b) show that there were more flux cancellation between n1 and s2 and more flux emergence in s1. Figure 6(c) shows that the average longitudinal field strength in s1 was all along stronger

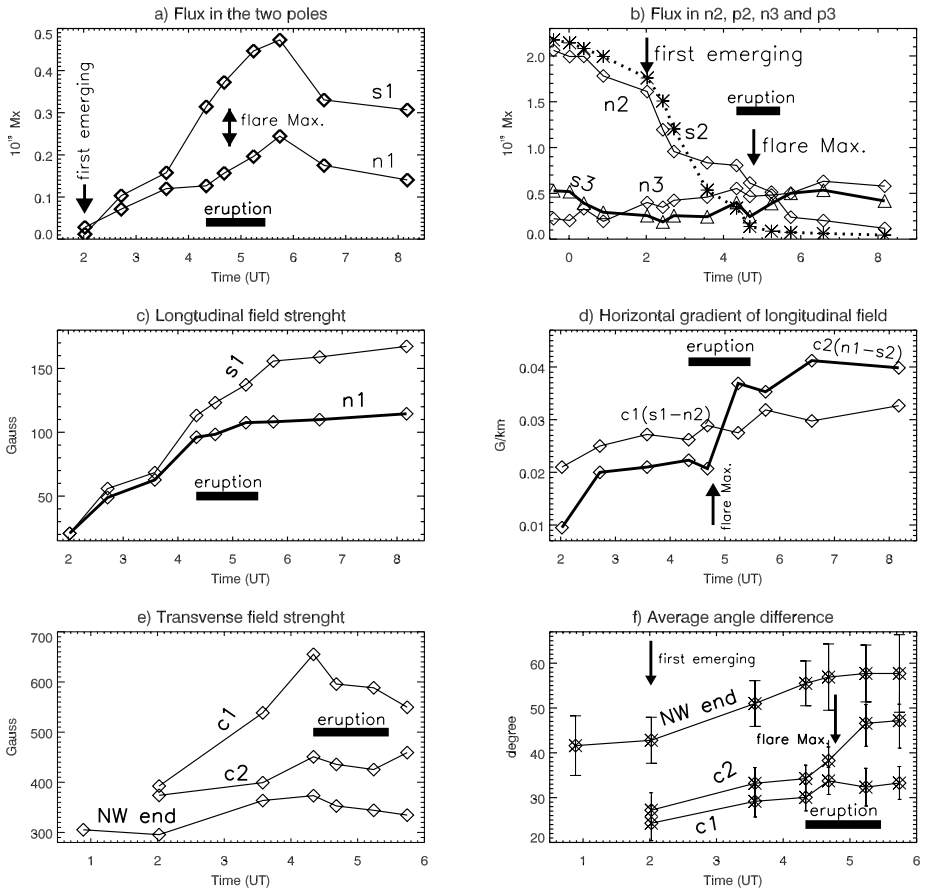

Fig. 6 Changes of magnetic flux in the two poles n1 and s1 (a), magnetic flux in the magnetic patches s2, n2, s3 and n3 (b), average longitudinal field strength of n1 and s1 (c), horizontal gradient of longitudinal field across the two short neutral lines in c1 and c2 (d), transverse field strength along the three neutral lines below the NW filament end and in c1 and c2 (e), and average angle difference between the three neutral lines above and the observed transverse field (f). For clarity, the absolute values for the negative fluxes are plotted in (a) and (b), and 3.4, 7.7, 1.8 and 3.5×10^{19} Max are subtracted from the flux values of s2, n2, s3 and n3 in (b), respectively. In (f), the error bars are plotted.

than that in n1. Across two short neutral lines formed in c1 and c2, the line-of-sight field horizontal gradient was measured within a distance of 2 arcsecs from the positive to negative polarity, and the changes of their average value are plotted in Figure 6(d). We see that, at time 6h, the field gradient increased faster in c2 than in c1. This also suggests that more violent flux cancellation was taking place in c2, which is consistent with the result shown in Figure 6(b). It is of interest to note that such increase in the field gradient steepened during the eruption.

The bipole emergence made the magnetic field evolution appear more complicated near the NW end of the filament. The neutral inversion line between n2 and s2 (the white curve in the first frame of Fig. 5(b)) was destroyed and shaped into a more strongly curved profile. The distribution of the transverse field near this filament end was strongly disturbed. A bundle of transverse field segment lying between the two poles appeared and slowly go stronger.

As shown in Figure 5(b), the transverse field had a nonpotential character at 00:53 UT, namely, it was aligned more or less parallel to the filament axis. At 05:44 UT, however, the transverse field was nearly perpendicular to the filament axis. Along the neutral inversion line between s2 and n2, we measured the absolute average value of transverse field strength and the average angle difference between the azimuths of the transverse field and the neutral line. The result is plotted in Figure 6(e) and 6(f) and labeled "NW end". We see that the transverse field strength and the angle difference had obvious enhancement after the bipole emergence.

It is clear that the emerging flux tube was topologically separated from the magnetic field of the filament and its overlying arcade. However, since L1 and L2 in the X-ray overlying the NW filament end were close to the two emerging poles, the obvious flux cancellation in the two CMFs implied a strong interaction between the footprints of the bipole and the arcade. As shown by Wang & Shi (1993), flux cancellation can be considered as a slow reconnection in the photosphere. The changes of transverse field in the two CMFs also suggested the occurrence of cancellation reconnection. Along the two neutral lines in c1 and c2, the average transverse field strength and the average angle difference between the observed transverse field and the neutral lines were measured. The results are also plotted in Figure 6(e) and (f) and labeled "c1" and "c2". These measurements all showed a tendency of continuous increase, which steepened before the eruption. This means an increased interaction between the bipole and the arcade, as well as a greatly decreased magnetic shear in their interface, hence an enhancement of magnetic connectivity between them. Thus, we think that a relatively fast reconnection occurred before the eruption. Such a cancellation reconnection could lead to the accumulation of magnetic flux and complexity in the filament via changing the magnetic tether of the filament to the photosphere, so was directly relevant to its sudden eruption. Therefore, it appears that the filament eruption was triggered by the emerging bipole. The interaction of the bipole with the arcade overlying the filament was the most important driving mechanism to destabilize the filament. It seems that cancellation reconnection between their footprints had occurred in the low atmosphere before the eruption.

5 CONCLUSIONS AND DISCUSSION

On 1997 April 9, the filament between the preceding and following parts of the sigmoidal active region, AR 8027, exhibited an obvious overall S-shape. A distinct bipole emerged in the filament channel, then a J-shaped part of the filament was activated and finally erupted. We have examined the morphological and dynamic evolution of the eruptive filament, and the associated changes of coronal structure and magnetic field in the filament channel. Our main results are summarized as follows:

(1) Before the eruption, the filament had been clearly disturbed. In the course of the eruption, it rose quickly and expanded laterally, and eventually the SE end detached from the chromosphere while the NW end remained fixed. Obvious helical structure and motion were seen in the filament body, and downward draining mass motion in the two ends. The filament survived the violent eruption but parts of it disappeared. After the eruption it slowly tended to quiescence.
(2) In the soft X-ray AR 8027 showed an S-shape morphology. Just before the eruption, first two loops arching across the filament brightened, then a bright string/rail structure lying exactly over the H_α filament and several cusped loops were observed. After the eruption, a bright arcade with a low-lying, axial spine/backbone structure was formed.

(3) The bipole began to emerge about 2.5 h before the eruption. It showed some typical features of EFR and its axis rotated counterclockwise. Two CMFs were formed between its two poles and the surrounding flux with opposite polarity, and substantial flux cancellation occurred in them. Moreover, the positive pole suffered more flux loss so only the negative pole showed up as a pore. Due to the bipole emergence the neutral inversion line below the NW filament end was severely deformed, and the transverse field alignment underwent large changes. It is strongly evident that pre-eruption cancellation reconnection occurred in the two CMFs, which was enhanced just before the eruption.

We attribute the eruption to the emerging bipole, since the eruption took place shortly after the bipole emerged while the flux emergence and cancellation were the solely observable changes of magnetic field in the whole filament channel. Unexpectedly, the NW end of the filament, below where the bipole emerged, persisted throughout the eruption. However, as suggested by Raadu et al. (1988), a small EFR with strongly concentrated magnetic field can trigger an eruption in a much large filament structure. Surprisingly too, the filament continued to exist after the violent eruption. This suggests that either the overall field configuration supporting the filament was not destroyed completely or a favorable condition for the maintenance was formed during the eruption. It is possible that the arcade was cut open only partially and not completely (McAllister et al. 1996), so the major part of the filament was still blocked below while some of the filament material escaped. The magnetic fields of a filament and its overlying arcade are considered as two separate parts of a large single magnetic system but can interact with each other (Martin 1998), and it is accepted that a flare is produced by magnetic reconnection of arcade elongated by erupting filament (Kopp & Pneuman 1976). Thus, the magnetic fields of the bipole, the filament and the overlying arcade were three different magnetic systems and the interaction among them can lead to the eruption. It is clear that the filament eruption with following subflare was an integral process coordinated by the emerging bipole. The key element of this eruption is that the flux cancellation in the two CMFs represents a slow pre-eruption reconnection in the interface of the bipole and the overlying arcade. This cancellation reconnection can change the linkage of the arcade to the photosphere so can alter the condition that restrains the arcade to the filament. As a result, the filament was disturbed and eventually erupted at a critical stage of flux cancellation.

Acknowledgements We are indebted to the staff at HSOS for making good observations. We thank the YOHKOH and EIT teams for data support. This work is supported by the National Natural Science Foundation of China (G10573033) and the National Key Research Science Foundation (2006CB806303).

References

Ai G., Hu Y., 1986, Pub. Beijing Astron. Obs., 8, 1
Canfield R. C., Hudson H. S., Mckenzie D. E., 1999, Geophys. Res. Lett., 26, 627
Delaboudiniére J. -P., et al., 1995, Sol. Phys., 162, 291
Deng Y., Ai G., Wang J., et al., 1997, Sol. Phys., 173, 207
Feynman J., Martin S. F., 1995, J. Geophys. Res., 100(A3) 3355
Filippov B. P., 1998, In: D. Webb, D. M. Rust, B. Schmieder, eds., IAU Colloq. 167, ASP Conference Series, p.342
Jiang Y., Wang J., 2000, A&A, 356, 1055
Jiang Y., Wang J., 2001, A&A, 367, 1022
Jiang Y. C., Li L. P., Yang L. H., 2006, Chinese. J. Astron. Astrophys. (ChJAA), 6, 345
Khan J. I., Uchida Y., McAllister A. H. et al., 1998, A&A, 336, 753
Khan J. I., Uchida Y., McAllister A. H., Watababe T., 1994, In: Y. Uchida, T. Watanabe, K. Shibata, H. S. Hudson, eds., X-Ray Solar Physics from Yohkoh, New York: Universal Academy Press, p.201
Kim J., Yun H. S., Lee S. et al., 2001, ApJ, 547, L85
Kano R., 1994, In: Y. Uchida, T. Watanabe, K. Shibata, H. S. Hudson, eds., X-Ray Solar Physics from Yohkoh, New York: Universal Academy Press, Inc., p.273
Kopp R. A., Pneuman G. W., 1976, Sol. Phys., 50, 85
Leka K. D., Canfield R. C., Maclymont A. N. et al., 1996, ApJ, 462, 547
Martin S. F., Livi S., 1992, In: Eruptive Solar Flares, Z. Sŭvestka, B. V. Jackson, M. E. Machado, eds., IAU Colloq. 133, Springer-Verlag, p.33
Martin S. F., 1998, Sol. Phys., 182, 107

McAllister A. H., Uchida Y., Tsunetaa S. et al., 1992, PASJ, 44, L205
McAllister A. H., Kurokawa H., Shibata K. et al., 1996, Sol. Phys., 169, 123
Moore R. L., Roumeliotis G., 1992, In Z. Švestka, B. V. Jackson, M. E. Machado, eds., IAU Colloq. 133, Springer-Verlag, p.69
Mouradian Z., Soru-Escaut I., Pojoga S., 1995, Sol. Phys., 158, 269
Mouradian Z., Soru-Escaut I., Hiei E. et al., 1998, Sol. Phys., 180, 313
Raadu M. A., Schmieder B., Mein M. et al., 1988, A&A, 197, 289
Romplt B., 1990, Hvar Obs. Bull., 14(1), 37
Rust D. M., Nakagawa Y., Neupert W. M., 1975, Sol. Phys., 41, 397
Rust D. M., Kumar A., 1996, ApJ, 464, L199
Schmieder B., Raadu M. A., Malherbe J. M., 1985, A&A, 142, 249
Schmieder B., Fontenla J., Tandberg-Hanssen E., 1991, A&A, 252, 343
Simon G., van Driel–Gesztelyi L., Schmieder B. et al., 1986, In: A. Poland, ed., CPP NASA Conference, C. P. 2442, p.229
Soberg F. C. R., McAllister A., 1998, In: D. Webb, D. M. Rust, B. Schmieder, eds., IAU Colloq. 167, ASP Conference Series, p.171
Sterling A. C., Hudson H. S., 1997, ApJ, 491, L55
Tandberg-Hanssen E., 1995, The Nature of Solar Prominences, Dordrecht: Kluwer Acad. Publ.
Tonooka H., Matsumoto R., Miyaji S. et al., 1998, In: T. Watanabe et al., eds., Observational Plasma Astrophysics: Five Years of Yohkoh and Beyond, Dordrecht: Kluwer Acad. Publ., p.371
Tsuneta S., Acton L., Bruner M. et al. 1991, Sol. Phys., 136, 37
Uchida Y., 1998, In: D. Webb, D. M. Rust, B. Schmieder, eds., IAU Colloq. 167, ASP Conference Series, p.163
Vršnak B., Ruždjak V., Rompolt B., 1991, Sol. Phys., 136, 151
Wang Y. -M., Sheeley N. R., Jr., 1999, ApJ, 510, L157
Wang J., Shi Z., 1993, Sol. Phys., 143, 119
Wang J., 1993, Publ. Beijing Astron. Obs., 19, 36
Wang J., Shi Z., Martin S. F., 1996a, A&A, 316, 201
Wang J., Shi Z., Wang H. et al., 1996b, ApJ, 456, 861
Zhang J., Wang J. X., Nitta N., 2001, Chin. J. Astron. Astrophys. (ChJAA), 1, 85
Zwaan C., 1987, Ann. Rev. Asrtophys., 25, 83